Applied Clay Science 241 (2023) 106997

Contents lists available at ScienceDirect

Applied Clay Science

journal homepage: www.elsevier.com/locate/clay

Research Paper

Adsorption and diffusion of selenite on Boda Claystone Formation

O. Czömpöly [a], M. Fábián [a], T.I. Korányi [a], G. Nagy [a], Z.E. Horváth [a], I. Zizak [b], S. Pollastri [c], M. Aertsens [d], J. Osán [a,*]

[a] Centre for Energy Research, Konkoly-Thege M. út 29-33, H-1121 Budapest, Hungary
[b] Helmholtz-Zentrum Berlin für Materialien und Energie GmbH, Department Structure and Dynamics of Energy Materials, Hahn-Meitner-Platz 1, 14109 Berlin, Germany
[c] Elettra Sincrotrone Trieste, Strada Statale 14 - km 163,5, I-34149 Basovizza, Trieste, Italy
[d] Belgian Nuclear Research Centre (SCK CEN), Boeretang 220, B-2400 Mol, Belgium

ARTICLE INFO

Keywords:
Boda Claystone Formation
Selenite mobility
Clay rich media
Diffusion
Adsorption

ABSTRACT

This study provides adsorption and diffusion data of selenite on Boda Claystone Formation (BCF) which is a potential host rock of a deep geological disposal of high-level radioactive waste. The experiments were performed on two diverse core samples: one albitic claystone sample characteristic for the entire BCF and one pyrite containing sample sparsely occurring in BCF. The experiments were carried out under atmospheric conditions. Batch experiments were carried out to study the kinetics of adsorption at a high initial concentration (1.2×10^{-3} M), the adsorption isotherms and reversibility were investigated in the 10^{-10}–10^{-3} M concentration range. Adsorption onto petrographic thin sections was done to study the elemental distribution on the microscale and the oxidation state of selenium. The maximum of the distribution coefficient was found as $K_d \approx 200$ L/kg and a decrease was experienced around 10^{-6}–10^{-7} M equilibrium concentration, which showed similarities to other argillaceous rocks. Isotopic exchange experiments revealed reversibility of selenite adsorption. Diffusion was studied with through-diffusion and in-diffusion experiments. Using X-ray fluorescence, despite a low initial concentration of 2.3×10^{-5} M in the in-diffusion experiment, a meaningful diffusion profile of selenium could be obtained, from which the selenite apparent diffusion coefficient $D_{app}^{selenite} = (1.5–4.3) \times 10^{-14}$ m^2/s and the selenite rock capacity factor $\alpha^{selenite} = 1.4–2.2$ were determined. As selenium species are redox sensitive the oxidation state of adsorbed species was studied with X-ray absorption near edge structure spectroscopy on Se—K edge. Adsorbed selenium remained in +IV oxidation state, however reduction was experienced on the pyritic sample.

1. Introduction

Deep geological repositories for high-level radioactive waste will have several engineering and natural barriers. As the disposal is designed for thousands of years, leakage of the facilities might occur during this time period. Migration across the natural barrier and in consequence our safety is determined by retardation of the released radioactive components. As natural barrier, clay rich rock media are considered as adequate host rocks due to their excellent retention capability of radionuclide components (as they have high adsorption capacity) (Dähn et al., 2002, 2021; Osán et al., 2014). Clay minerals have negative charges which are compensated by adsorption of cations (Tertre et al., 2021). Due to this phenomenon, clay minerals have high cation exchange capacity.

The safety of repositories is evaluated with performance assessment (PA) analysis which tries to predict the consequences of a possible radionuclide (RN) escape from the waste packages. Retention characteristic of the host rock is a crucial parameter during PA analysis. Selenium-79 is a fission product in nuclear reactors and considered as a key nuclide due its long half-life ($3.27 \cdot 10^5$ a), toxicity and its anionic chemical form (Puranen et al., 2009). Depending on the geochemical properties, selenium could be found mainly in five different forms after a leakage: selenide (Se^{2-}), Se^-, elemental selenium (Se), selenite (SeO_3^{2-}) and selenate (SeO_4^{2-}). The different forms can coexist in equilibrium in the systems. Selenide and elemental selenium form precipitation at the conditions being present in the geochemical systems, selenium oxyanions are soluble in aqueous systems. Former studies showed that selenate sorbs very weakly in clay-rich media and it is less sensitive for redox reactions than selenite (Aurelio et al., 2010; De Cannière et al., 2010; He et al., 2019). The difference between the redox sensitivity of

* Corresponding author.
E-mail address: osan.janos@ek-cer.hu (J. Osán).

https://doi.org/10.1016/j.clay.2023.106997
Received 3 February 2023; Received in revised form 11 May 2023; Accepted 12 May 2023
Available online 17 May 2023

selenite and selenate were explained by an intermediary Se(V) barrier which prevents the reduction of selenate (Bailey, 2016; Kläning and Sehested, 1986; Séby et al., 2001; Tian et al., 2020). In contrary selenite reduction to elemental selenium and selenide was experienced in the presence of pyrite (FeS_2) and organic matter in various studies (Bailey, 2016; Bruggeman et al., 2005; Savoye et al., 2021).

Once the integrity of the radioactive waste containers is damaged, the RNs need to pass through the buffer material around the waste packages before reaching the natural barriers. The rate of the RN transport process is characterized by the apparent diffusion coefficient (D_{app}) and the rock capacity factor α. Several studies were conducted on the adsorption properties of selenium species but regarding diffusion less data are available in the literature. H. Wu et al. (2020) conducted their experiments with selenite on compacted Tamusu clay by capillary method, De Cannière et al. (2010) studied selenate diffusion in Boom Clay, where they reported a diffusion coefficient of selenate very similar to sulfate. Recently the main focus regarding selenium diffusion was on Callovo-Oxfordian clay (COx). Both Savoye et al. (2021) and Descostes et al. (2008) investigated the diffusion properties of selenite with through-diffusion experiments under anoxic conditions.

Boda Claystone Formation (BCF) (Fedor et al., 2019) is considered a potential host rock for high-level radioactive waste repository in Hungary. It has total clay mineral content similar to other widely studied clay formations e.g. COx and Opalinus clay (OPA), meanwhile it has unique features since it is the oldest in Europe (265 Ma) and it has an over-consolidated, highly indurated character with low physical porosity ($\varepsilon_{tot} \approx 0.02$) (Nuclear Energy Agency (NEA), 2022; Sámson, 2015). As the early diagenesis of BCF occurred in oxidative environment, most of the studies regarding the migration of RNs in BCF were investigated under atmospheric conditions previously (Gergely et al., 2016; Marques Fernandes et al., 2015; Mell et al., 2006). To our knowledge studies regarding selenium retention and migration in BCF has not been published. The present study investigated the adsorption and diffusion properties of selenite in BCF under atmospheric conditions. In the pores of the buffer and backfill materials in radioactive waste repositories O_2 is present after construction and decreases based on the consumption rate of O_2. Moreover, initially the moisture content could be insufficient to saturate the entire buffer/backfill. The conditions of the repository environment can be addressed with four possibilities: (i) in the early life aerobic and unsaturated which at some point becomes (ii) saturated, however during the evolution of repository conditions (iii) unsaturated/ (iv) saturated anaerobic conditions can coexist with aerobic phases. Adsorption and diffusion experiments at atmospheric conditions can provide valuable input for PA regarding an early failure of the repository.

The aim was to study the adsorption in wide concentration range, to determine the diffusion parameters and to verify the oxidation state of adsorbed selenium. Since many European countries consider argillaceous host rocks for deep geological repository, the obtained results were discussed in comparison to those reported for other clay rich rock systems.

The properties of BCF regarding selenite adsorption species were studied using an albitic claystone sample which is the most characteristic rock of the formation. Some experiments were carried out also with a pyrite containing sample originating from a unique layer formed under reductive environment. Radiotracer method was applied to obtain the adsorption isotherm in the 10^{-10}–10^{-3} M range and to study the reversibility of adsorption for crushed rock samples. Adsorption experiments with inactive selenite involving petrographic thin sections aimed to find the minerals responsible for selenium uptake. In- and through-diffusion experiments on compact rocks were carried out using only inactive selenite. Microscale elemental distributions and selenium diffusion profiles along the diffusion axis were collected using microscopic X-ray fluorescence. Because of the moderate adsorption of selenite oxyanion onto clays, synchrotron radiation was applied. The oxidation state of the adsorbed selenium was studied applying X-ray absorption spectrometry.

Table 1
Mineral (Table 1/a) and oxide (Table 1/b) composition of studied rocks in m/m % (Sámson, 2015). In Table 1/b LOI (loss of ignition) means the mass loss in % experienced during heating the sample above 1050 °C for 2 h, TOC stands for total organic carbon content.

Component	Sample A	Sample P
a.		
Vermiculite	2	3
Illite	24	13
Chlorite	6	31
Quartz	7	18
Pyrite	<1	2
Albite	43	26
K-feldspar	<2	<2
Calcite	5	3
Dolomite	8	4
Hematite	6	<1
b.		
SiO_2	49.2	50.2
Al_2O_3	16.0	16.1
$Fe_2O_{3\ total}$	7.8	7.4
FeO		3.9
$FeO_{\ total}$		6.6
Fe_2O_3		3.0
MgO	4.3	6.1
CaO	4.8	3.50
Na_2O	3.1	3.6
K_2O	4.5	2.8
MnO	0.14	0.14
TiO_2	0.84	0.81
CO_2	4.3	3.2
P_2O_5	0.31	0.17
LOI	8.3	8.5
TOC	0.11	0.24

2. Materials and methods

2.1. Characteristics of BCF

The studied rocks were geochemically characterized, drilled core samples from BCF. The formation is located in West-Mecsek Mountains, Hungary where two distribution areas are known the perianticlinal structure of Boda Block (BB) and the Gorica Block (GB). BCF sediments are red, reddish-brown colored testifying the oxidizing nature of the early diagenetic and depositional environments (Fedor et al., 2019; Hrabovszki et al., 2020). Up to now one reductive interbedding is known (greyish colored) with a thickness of 3–4 m containing pyrite. The deposition of BCF occurred about 265 Ma ago in a shallow-water salt lake environment in the neighboring of saline mudflat under arid climatic conditions (Árkai et al., 2000; Lázár et al., 2012; Varga et al., 2005). The catagenetic stage was reached under high temperature (200–250 °C) and pressure (120–150 MPa) conditions during sedimentation. During the Cretaceous Period, the formation was covered by sediments of up to 3.5–4.5 km thickness. This burial and compaction resulted in an over-consolidated, highly indurated character of BCF (Nuclear Energy Agency (NEA), 2022). BCF is highly heterogeneous both on the macro and the microscale. The main minerals being present are clay minerals (10–55 m/m%), authigenic albite (20–60 m/m%), analcime, detrital quartz (5–30 m/m%), carbonate minerals (calcite and dolomite, 10–50 m/m%) and hematite (5–10 m/m%) (Fedor et al., 2019; Sipos et al., 2010; Varga et al., 2006). On the microscale two significant areas should be mentioned: the main clayey matrix and the minor fracture and vug infillings. The clayey matrix is formed of albite cement (and analcime cement for GB) and several clay minerals (mainly phyllosilicates, as illite (15–50 m/m%) chlorite (0–35 m/m%), smectite, kaolinite, vermiculite and mixed structure minerals can be found in

Table 2
Composition of Boda synthetic porewater in equilibrium with atmospheric CO_2 partial pressure (Breitner et al., 2015).

Element	Concentration (M)
Na	$1.7{\cdot}10^{-2}$
K	$1.8{\cdot}10^{-4}$
Mg	$2.4{\cdot}10^{-3}$
Ca	$3.1{\cdot}10^{-3}$
Cl	$2.3{\cdot}10^{-2}$
CO_3^{2-}/HCO_3^-	$6.1{\cdot}10^{-4}$
SO_4^{2-}	$1.9{\cdot}10^{-3}$
Si	$1.8{\cdot}10^{-4}$

inconsiderable amounts (Fedor et al., 2019)). In the greyish interbedding the presence of illite decreases and chlorite becomes the major clay mineral being present. Illite is the most important clay mineral with a high potassium and iron content (Mills et al., 2023). Hematite nanocrystals were detected between illite crystallites in albitic claystone with transmission electron microscopy (Németh et al., 2016). The major components of fracture and vug infillings are authigenic albite (25–45 m/m%), quartz, carbonates and hematite. Overall, the most dominant rock type of BB is albitic claystone while in the GB is albite and analcime-bearing claystone (Konrád et al., 2010). The BCF rocks investigated in this study belong to the BAF-2 borecore deepened in BB including both albitic claystone and the reductive interbedding from depths of 324.52–324.71 m (Sample A) and 151.62–152.12 m (Sample P), respectively. The bulk dry density of BCF samples is between 2700 and 2800 kg/m^3, the cation exchange capacity varies between 100 and 150 cmol(+)/kg (Marques Fernandes et al., 2015). Main mineral and elemental composition, and total organic carbon content as provided with the samples by the Public Limited Company for Radioactive Waste Management (PURAM, Hungary) can be found in Table 1a-b (Sámson, 2015).

Diffusion values (D_e and ε) for tritiated water (HTO) and Cl^- have been already studied and published for BCF (van Loon and Mibus, 2015). For HTO, the effective diffusion coefficient is $D_{eff}^{HTO} = (1.17 \pm 0.02) \times 10^{-11}$ m^2/s, for Cl^- $D_{eff}^{Cl^-} = (3.95 \pm 0.24) \times 10^{-13}$ m^2/s, anion accessible porosity was found to be 0.03 ± 0.002, meanwhile the total porosity for HTO has been reported as $\varepsilon_{tot} = 0.076 \pm 0.005$ (van Loon and Mibus, 2015). One should note that these values were obtained for a different rock section of BCF, but they can be considered as a good estimate for BAF-2 albitic claystone. The BCF heterogeneity might also explain the much lower value $\varepsilon_{tot} \approx 0.02$ of Sámson (2015).

2.2. Sample preparation

For through-diffusion experiment a slice with a thickness of 5.6 mm was cut and polished from the full 62 mm diameter core of Sample A. Petrographic thin sections with an average thickness of 50 μm were prepared from sample A onto high purity silicon wafers for adsorption experiments. Cutting of full-core slices was not possible from Sample P, for this reason a $1.03 \times 1.04 \times 2$ cm^3 cuboid was cut that could only be used for in-diffusion experiment. For performing batch adsorption experiments 50 g of each rock sample was crushed and sieved below 63 μm particle diameter. Prior to the launch of experiments both crushed and compact rocks were conditioned with synthetic porewater at pH 8.0 ± 0.1 based on the method of Marques Fernandes et al. (2015). Because of the low porosity, only formation water was available for BCF, therefore the chemical composition of the pore water (Breitner et al., 2015) (Table 2) was calculated to be in equilibrium with atmospheric p_{CO2}, and under the constraint of calcite, dolomite and quartz saturation (Bradbury and Baeyens, 1998). TRIS (tris(hydroxymethyl)aminomethane) was applied as a pH buffer at 2 mM concentration.

2.3. Adsorption experiments

Adsorption experiments were carried out in both dispersed (crushed rocks) and in compacted (thin sections) forms under atmospheric conditions. After addition of sodium selenite to the synthetic porewater the pH was readjusted to 8.0 ± 0.1. Measurements of the initial speciation of selenium was performed with ion chromatography (Thermo Scientific Dionex Aquion equipped with AS 23 column and 4.5 mM Na_2CO_3/ 0.8 mM $NaHCO_3$ eluent). Selenium was present in selenite form in 96% meanwhile 4% of the selenium was found as selenate. The adsorption results were corrected for the selenate concentration. Savoye et al. (2021) reported the presence of selenate around 6% in the radiotracer they applied, they explained the speciation change by radiolysis processes.

2.3.1. Kinetic studies

As a first step the kinetics of adsorption was studied with batch experiments to determine the required time to reach quasi-equilibrium of adsorption. The applied liquid-to-solid ratio (V/m) was 100 mL/g and 50 mL of the selenite containing synthetic porewater together with 0.50 g of crushed and conditioned rock were introduced into 100 mL shaker vessels, then put onto an orbital shaker for 28 days (Ohaus SHHD1619AL). The experiments were performed with Sample A and the initial selenite concentration was 1.2×10^{-3} M. The concentration of the solutions was monitored with ICP-OES (Perkin Elmer Avio 200).

2.3.2. Adsorption isotherm

To obtain the adsorption isotherm for sample A, solutions with 10^{-10} M to 10^{-3} M concentration of selenite (using sodium-selenite) were prepared. The initial concentrations were checked using ICP-OES until the limit of detection (approximately 10^{-7} M for selenium). ^{75}Se radionuclide ($Na_2^{75}SeO_3$ in aqueous solution, POLATOM) was used as a tracer and solutions were spiked with 20 kBq of ^{75}Se in the whole 10^{-3} M - 10^{-10} M range. For each concentration two replicates of 0.50 g conditioned, crushed rock were added to 100 ml vessels with 50 ml solution containing selenite and shaked for 28 days. After reaching equilibrium with batch experiments the suspensions were separated using 220 nm syringe filters. The activity of initial and final liquid phases was measured in the same batch by liquid scintillation counter (LSC) (Perkin Elmer Tri-Carb with Ultima Gold scintillation cocktail).

In addition, for the high concentration range the sorption of selenite was also analysed by measuring the inactive Se concentration (with ICP-OES) after equilibration for 28 days. This was done for samples A and P (two replicates per concentration).

The results are shown in the form of distribution coefficient, K_d, which can be calculated using Eq. (1):

$$K_d = \frac{C_{in} - C_{eq}}{C_{eq}} \bullet \frac{V}{m} \tag{1}$$

where C_{in} and C_{eq} are the initial and equilibrium concentrations (in case of ICP-OES mol/L, in case of LSC counts/50 μL), V is the volume of the liquid phase (mL) and m is the mass of clay (g). Adsorption onto the wall of shaker vessels was studied and found negligible (below 1%).

Experimental data of the adsorption isotherm of sample A was fitted with the two-site Langmuir isotherm model (Eq. (2)). The fitting was carried out with OriginLab 2022b software.

$$C_s = S_{max,1} \frac{K_{L,1} \cdot C_{eq}}{1 + K_{L,1} \cdot C_{eq}} + S_{max,2} \frac{K_{L,2} \cdot C_{eq}}{1 + K_{L,2} \cdot C_{eq}} \tag{2}$$

where C_s is the amount of selenite adsorption onto solid phase (mol/kg), $S_{max,i}$ ($i = 1, 2$) is the adsorption capacity of site i (mol/kg), $K_{L,i}$ is the adsorption potential of site i (L/mol) and C_{eq} is the equilibrium concentration (mol/L).

Inactive suspensions of 10^{-5}, 10^{-4} and 10^{-3} M initial selenite concentration prepared from Sample A were filtered and washed, then

pellets were pressed to study the oxidation state of adsorbed selenium on crushed claystone.

2.3.3. Isotopic exchange experiments

To study the reversibility of adsorption suspension containing 0.50 g of crushed and conditioned rock of Sample A was added to 50 ml solution with varying selenite concentrations from 10^{-8}–10^{-3} M in duplicate. The suspensions were shaken for 28 days, afterwards 5 ml of the suspensions were taken from the shaking bottles and filtered with 220 nm syringe filter. Its concentration was determined with ICP-OES. Radiotracer (20 kBq of $^{75}SeO_3^{2-}$) was added to the remaining suspensions in equilibrium with inactive sodium selenite. Right after radiolabeling, 5 ml initial sample was taken and filtered. After 28 days, LSC counting was performed on liquid phases of both the initial suspensions and those equilibrated with ^{75}Se. The adsorbed fractions were calculated both for the inactive and active Se and compared for determining the reversibly adsorbed part of selenite, similarly to Rahman et al. (2019) used for assessment of As sorption reversibility in soils.

2.3.4. Elemental distribution of selenium on thin sections

Two petrographic thin sections of sample A were immersed into selenite containing porewater (10^{-4} and 10^{-3} M) for the same duration as batch experiments. After 28 days the thin sections were washed with ultrapure water and dried in vacuum. The lateral distribution of selenium and rock-forming elements was studied with μ-XRF mapping, while the oxidation state of selenium was investigated with (μ-)XANES.

2.4. Analysis of adsorbed selenium using synchrotron-based techniques

X-ray fluorescence (XRF) and X-ray absorption spectroscopy (XANES) measurements were performed at two beamlines. At Bessy-II synchrotron (Berlin, Germany) mySpot beamline μ-XRF and μ-XANES measurements were performed (Zizak, 2016). The beam was focused with polycapillary optics to 20 μm spot size. The measurements were performed on thin sections at 45°/45° geometry using a silicon drift detector (SDD) of 100 mm^2 active area. At Elettra synchrotron (Trieste, Italy) measurements both on pressed pellets and thin sections were performed at the XRF beamline (Karydas et al., 2018). In this case the focusing optics provide a quite large beam of roughly 500 × 300 μm^2 (H × V), whose size can be furtherly reduced by using exit slits. For the pressed pellets, the full beam was employed whereas for the thin sections a 450 × 50 μm^2 sized beam with shallow angle illumination was used to gain spatial resolution to study the diffusion profile in the rock. After obtaining the diffusion profile, XANES measurements were performed on selected points (for which the slits were fully opened). For XANES measurements Si(111) monochromators were applied at both beamlines. As selenite is present in the samples in very low amounts the excitation energy for XRF mapping was set to the peak of the white line (12,664 eV) of its X-ray absorption spectrum.

2.5. Diffusion experiments

For the through-diffusion experiment, a diffusion cell made of polycarbonate was applied (Mell et al., 2006). The claystone section divides the cell into upstream and downstream reservoirs with a volume of 165 mL each (Fig. S1a in Supplementary Material) and a clay surface of 19.64 cm^2. The claystone slice was glued in the cell then the two sides were screwed together. No filter was applied due to the very limited swelling of Boda claystone. After installing the diffusion cells both reservoirs were filled by synthetic porewater to saturate the BCF core disc. During the 6-week conditioning the solutions were changed every 2 days. The through-diffusion experiment was conducted at an initial concentration of 10^{-3} M of inactive sodium-selenite on a 62 mm diameter 5.6 mm thick slice of Sample A. The effective diameter available for diffusion was 50 mm. After finishing the experiment, the cell was disassembled, a piece of 5 × 10 × 5.6 mm^3 was cut from the centre of the claystone disc and a petrographic thin section was prepared for X-ray spectroscopy measurements.

Regarding the in-diffusion experiment a 3D printed sample holder was applied (Fig. S1b). With a threaded rod the height of the cuboid from sample P could be manipulated in a way that only the bottom surface touched the liquid surface. The experiment was performed in a closed container with 100 ml porewater with an initial selenium concentration of 2.3 × 10^{-5} M for 87 days. The clay surface was 1.07 cm^2. After finishing the experiment, a petrographic thin section was prepared for post-mortem analysis.

2.6. Applied models for diffusion

Diffusion is described by the diffusion equation

$$\frac{\partial C}{\partial t} = D_{app}\frac{\partial^2 C}{\partial x^2} \tag{3}$$

where C (x,t) is the concentration (mol/m^3 or counts/m^3), x is the position (m), t is time (s) and D_{app} stands for the apparent diffusion coefficient (m^2/s). In porous media, diffusion is characterized by two parameters: the apparent diffusion coefficient D_{app} and the rock capacity α (−). For retarded species, the rock capacity α is related to the distribution coefficient K_d (m^3/kg) by

$$\alpha = \varepsilon_{tot} + \rho K_d \tag{4}$$

where ε_{tot} is the total porosity (−) and ρ (kg/m^3) the dry bulk density. In that case, the retardation coefficient R is the ratio $R = \alpha/\varepsilon_{tot}$ with $R > 1$. For unretarded species,

$$\alpha = \varepsilon \tag{5}$$

with ε (−) the accessible porosity ($\varepsilon \leq \varepsilon_{tot}$). The effective diffusion coefficient D_{eff} (m^2/s) is the product αD_{app} ($D_{eff} = \alpha\, D_{app}$).

For modelling, the diffusion equation is solved numerically by COMSOL coupled with MATLAB for optimization.

The background Se concentration in Boda Claystone (1.3 ± 0.3 mg/kg corresponding to (1.7 ± 0.4) × 10^{-5} mol/kg) is considered sufficiently low to neglect (see Fig. 3). Because in the through-diffusion experiment, neither the upstream nor the downstream reservoir are replaced, basically the VC-VC (Variable Concentration upstream and downstream) case (Takeda et al., 2008) is solved. In case the upstream and downstream compartments are sufficiently large, the VC-VC case is approximated well by the CC-CC (Constant Concentration upstream and downstream with the upstream concentration C_0 much higher than the downstream concentration) case (Takeda et al., 2008). Here, after a sufficiently large time a quasi-stationary state is reached, and the concentration $C_{down}(t)$ in the downstream volume is given by (e.g. Aertsens, 2011)

$$C_{down}(t) = \alpha\, C_0 \left(\frac{D_{app} t}{L^2} - \frac{1}{6}\right) \tag{6}$$

where L is the clay core length (m) ($L = 5.6$ mm). This expression is valid only for not too large times (to remain consistent with the basic assumption $C_{down} << C_0$) and the breakthrough time τ (defined by $C_{down}(\tau) = 0$) is determined by the apparent diffusion coefficient:

$$\tau = \frac{L^2}{6\, D_{app}} \tag{7}$$

The through-diffusion experiment is modelled in two ways:

- assuming a single Se species: the evolution of the Se concentration in the downstream compartment is fitted as a function of time leading to $D_{app,Se}$ and α_{Se}. Next these values are used to estimate the Se concentration (*i*) in the upstream compartment, and (*ii*) in the clay core, and compared to the experimental data.

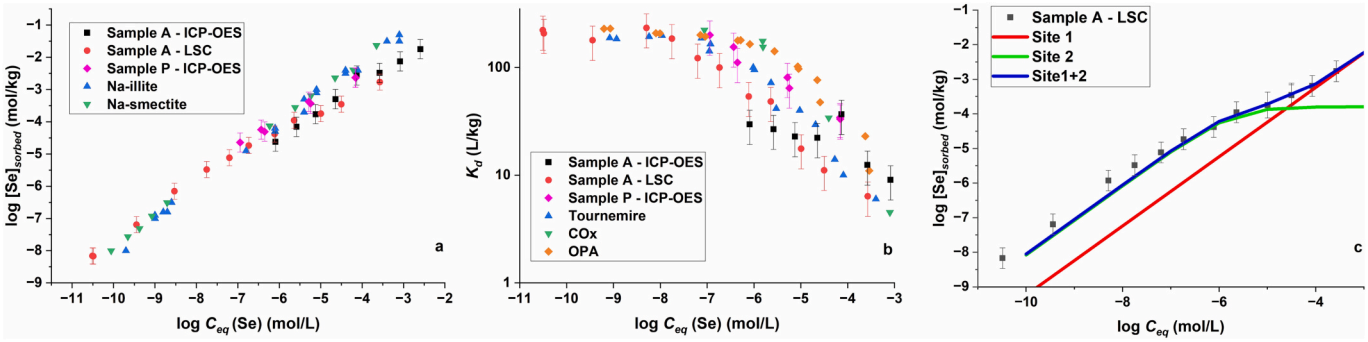

Fig. 1. Adsorption isotherm of selenite on BCF and pure clay minerals on panel (a) (Na-illite, Na-smectite) (Missana et al., 2009) and other argillaceous rocks on panel (b) (Tournemire, Callovo-Oxfordian and Opalinus clay) (Frasca et al., 2014). LSC and ICP-OES stand for the applied method to measure the initial and equilibrium activities and concentrations. On panel (c) the calculated contributions of the Langmuir sorption sites are plotted with the measured data for Sample A.

- assuming two Se species: a fast-diffusing species Se_{fast} (assumed selenate) and a slowly diffusing species Se_{slow} (assumed selenite). The total Se concentration C_{S_e} is the sum of the concentrations of both species:

$$C_{Se} = C_{Se,fast} + C_{Se,slow} \quad (8)$$

In agreement with the speciation calculations, the initial upstream concentrations $C_{0,fast}$ (resp. $C_{0,slow}$) of the fast (resp. slow) Se species are taken as

$$C_{0,fast} = 0.04\ C_0;\ C_{0,slow} = 0.96\ C_0 \quad (9)$$

with C_0 the initial total Se concentration in the upstream compartment.

Both Se species are assumed to diffuse independently from another in the clay according to their diffusion parameters: $D_{app,fast}$, α_{fast}, $D_{app,slow}$ and α_{slow}. The values of $D_{app,fast}$ and α_{fast}, are fitted from the downstream evolution. Next, these values are used to estimate $C_{Se,fast}$ in the upstream volume and in the clay core. From the difference $C_{se,bulk} - (\alpha_{fast}C_{fast}/\rho)$ with $C_{se,bulk}$ the experimentally measured bulk concentrations and the wet and dry clay bulk densities assumed equal (justified by the very low total porosity of Boda clay), the values of $D_{app,slow}$ and α_{slow} are fitted, allowing to assess $C_{Se,slow}$. Finally, by expression (8) the concentration C_{Se} can be evaluated in both upstream and downstream compartment as a function of time and compared to the experimental data.

For the in-diffusion experiment the Se evolution in the upstream compartment was not measured. Only a single Se species is assumed, and the diffusion parameters of this species are estimated from fitting the Se profile in the clay core. Clearly, this species corresponds to Se_{slow}.

3. Results and discussions

3.1. Adsorption results

3.1.1. Results of kinetic tests

The kinetics of adsorption experiment was plotted in Fig. S2, the saturation curve reached its maximum below 10 days. Missana et al. (2009) reported a similar kinetic property of sodium-selenite adsorption onto Na-illite and Na-smectite under atmospheric conditions at a very low initial concentration (10^{-10} M). Their results showed that 7 days of contact time was sufficient to reach equilibrium. Savoye et al. (2021) studied the adsorption properties of selenite onto Callovo-Oxfordian (COx) rock samples. They carried out the experiments in a N_2/ 0.4% CO_2 glovebox at different concentrations, where at the high concentration region (10^{-4}–10^{-3} M) K_d reached equilibrium in 20 days, however at lower concentrations slower kinetic took place, so they decided to obtain the adsorption isotherm after 110 days of contact time. There is no clear evidence for the differences in the time needed to reach saturation in the mentioned experimental set-ups. After all, in the present study suspensions and thin sections were shaken and immersed for 28 days.

Table 3
Results of adsorption isotherm fitting with Langmuir parameters for BCF Sample A together with data published by Frasca et al. (2014) for Upper Toarcian, Black Shales and Opalinus Clay.

	S_{max1} (mol/kg)	K_{L1} (L/mol)	S_{max2} (mol/kg)	K_{L2} (L/mol)
Sample A	$1.9{\cdot}10^{-3}$	$4.4{\cdot}10^{3}$	$1.2{\cdot}10^{-4}$	$8.37{\cdot}10^{5}$
Upper Toarcian	$6.5{\cdot}10^{-4}$	$1.6{\cdot}10^{5}$	$2.9{\cdot}10^{-5}$	$1.3{\cdot}10^{7}$
Black Shales	$5.4{\cdot}10^{-4}$	$7{\cdot}10^{5}$	$2.6{\cdot}10^{-5}$	$2.2{\cdot}10^{7}$
OPA	$1.7{\cdot}10^{-3}$	$2.1{\cdot}10^{5}$	$1.4{\cdot}10^{-5}$	$1.9{\cdot}10^{7}$

3.1.2. Adsorption isotherm

The obtained adsorption isotherm of Sample A (Fig. 1) was compared to the ones measured with pure minerals. The maximum of K_d (200 L/kg) was found in the low concentration regime (10^{-10}–10^{-8} M). Around 10^{-6} M ($K_d \approx 100$ L/kg) the isotherms started to part away and the amount of selenite adsorbed to BCF had one order of magnitude lower value. In the high concentration range (10^{-6}–10^{-3} M) adsorption experiments were carried out on both sample A and sample P. In this concentration range Sample P had higher selenite adsorption than the albitic sample. In the low concentration region, below 10^{-6} M, similar results were found to those obtained for Na-illite and Na-smectite (Missana et al., 2009). Similarly to different argillaceous rocks (Frasca et al., 2014; Savoye et al., *2021*), a decrease compared to pure minerals started around 10^{-7}–10^{-6} M concentration, however the adsorption isotherm belonging to BCF appeared to have even lower K_d value (Fig. 1b). In previous studies the breakpoint in the isotherm was explained by the saturation of the adsorption sites. The lower K_d value of BCF corresponds to the higher argillite content of the compared rocks. The studied OPA and Tournemire samples contained around 60% of clay minerals (Frasca et al., 2014), meanwhile the mineralogy of the COx sample characteristic of its depth of origin contains around 35–65% argillite (Savoye et al., 2021). In contrary sample A has an illite and chlorite content altogether of 30–35% and sample P has around 40–45% of clay minerals. The lower selenite adsorption of Sample A than Sample P cannot be explained only by the difference in the clay mineral content. Despite the low TOC content (0.22 m/m%) of Sample P, the K_d values were more similar to other studied clays evolved under reductive conditions.

The results of the Langmuir isotherm fitting are presented in Table 3, the plot of the fit is shown in Fig. 1c. The goodness of fit for the present study can be characterized with $R^2 = 0.99973$, reduced Chi-square $= 8.21 \times 10^{-11}$. In the current study two sorption sites with different properties fit the sorption isotherm sufficiently well, one site with high capacity but low affinity and a low capacity but high affinity site. Frasca et al. (2014) also found that a two-site Langmuir model is in better

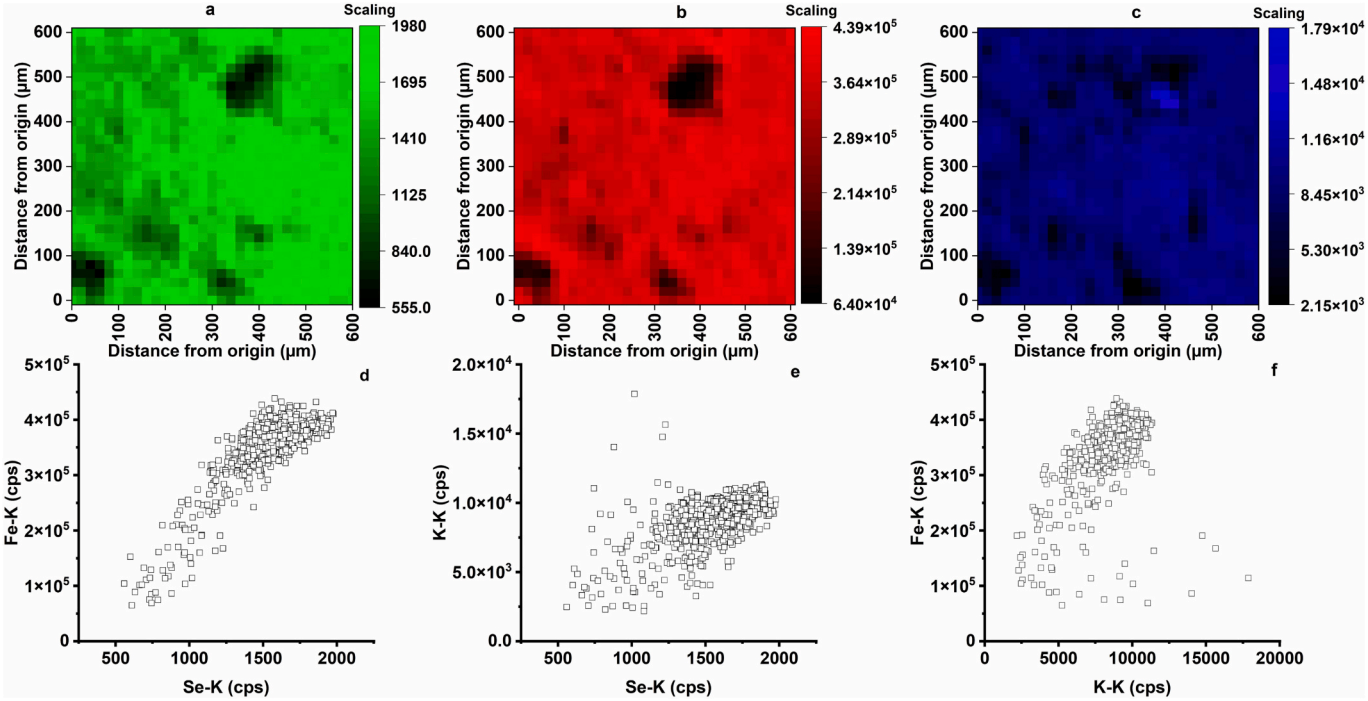

Fig. 2. Elemental distribution of Fe (panel (a)), K (panel (b)) and Se (panel (c)) on a petrographic thin section prepared from sample A obtained using µ-XRF. The initial concentration of Na-selenite was 10^{-3} M. On panel (d), (e), (f) scatter plots of Fe-K/Se-K, K-K/Se-K and K-K/Fe-K count rates, respectively.

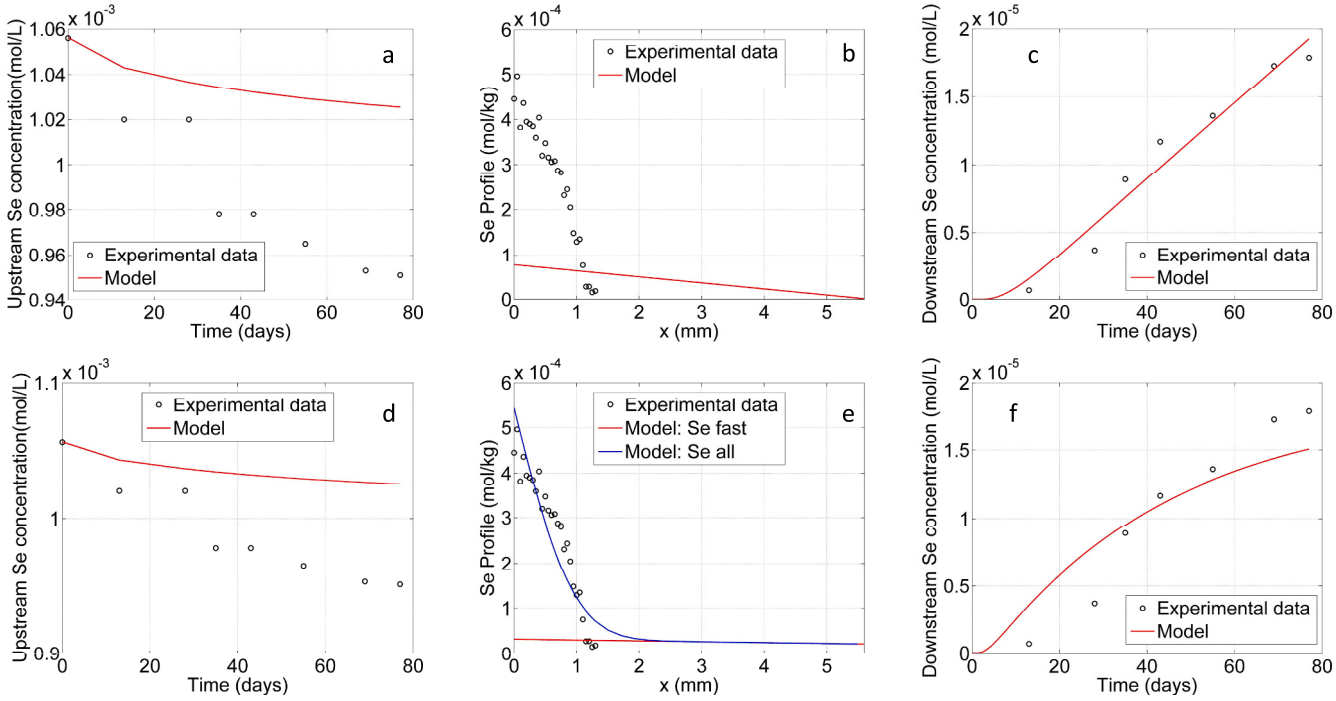

Fig. 3. Through-diffusion experiment (sample A): experimental data and model assuming a single diffusing Se species (top, panels a,b,c) and two diffusing Se species (Se_{fast} and Se_{slow}, bottom, panels d,e,f).
On panels a and d: Se concentration in the upstream compartment and model (data measured by ICP-OES).
On panels b and e: Se profile in the clay core at the end of the experiment and model (data from shallow angle illumination XRF).
On panels c and f: Se concentration in the downstream compartment and model (data measured by ICP-OES).
For the single Se species (top, panels a,b,c), the diffusion parameters are fitted from the downstream evolution and used to predict the upstream evolution and the Se profile in the clay at the end of the experiment. For two diffusing Se species (bottom, panels d,e,f), the diffusion parameters of selenate are fitted from the downstream evolution. These values are used to predict the selenate profile in the clay and from the difference with the experimental data, the diffusion parameters of selenite are estimated. The upstream evolution is predicted with the diffusion parameter values of selenate and selenite. The predicted downstream concentration of selenite is zero.

Table 4
Summary of the Se diffusion parameters. The distribution factor K_d is calculated by assuming $\varepsilon_{tot} = 0.02$ and $\rho = 2.7$ kg/L.

		C_0	D_{app}			α			D_{eff}			R	K_d
		(mol/L)	(m^2/s)			(−)			(m^2/s)			(−)	(L/kg)
Through-diffusion													
Se (all)	C_0	$1.06{\cdot}10^{-3}$	$7.2{\cdot}10^{-12}$	±	$4.3{\cdot}10^{-12}$	0.21	±	0.15	$1.5{\cdot}10^{-12}$	±	$1.4{\cdot}10^{-12}$	10	0.07
Se_{fast}	$C_{0,fast}=0.04C_0$	$4.22{\cdot}10^{-5}$	$1.5{\cdot}10^{-11}$	±	$4.7{\cdot}10^{-11}$	4.44	±	20.60	$6.7{\cdot}10^{-11}$	±	$3.7{\cdot}10^{-10}$	222	1.61
Se_{slow}	$C_{0,slow}=0.96C_0$	$1.01{\cdot}10^{-3}$	$4.3{\cdot}10^{-14}$	±	$4.4{\cdot}10^{-15}$	1.44	±	0.11	$6.1{\cdot}10^{-14}$	±	$7.90{\cdot}10^{-15}$	72	0.52
Se_{slow}	$C_{0,slow}=C_0$	$1.06{\cdot}10^{-3}$	$3.1{\cdot}10^{-14}$	±	$2.4{\cdot}10^{-15}$	1.95	±	0.24	$6.0{\cdot}10^{-14}$	±	$8.70{\cdot}10^{-15}$	98	0.70
In-diffusion													
Se_{slow}		$2.30{\cdot}10^{-5}$	$1.5{\cdot}10^{-14}$	±	$2.0{\cdot}10^{-15}$	2.22	±	0.16	$3.3{\cdot}10^{-14}$	±	$5.00{\cdot}10^{-15}$	111	0.80

agreement with their experimental data with $^{75}SeO_3^{2-}$ on OPA, Black Shales and Upper Toarcian Clays (Table 3). The site capacities of the other clay-rich rocks seem to be lower than or similar to those of BCF Sample A, however the affinity values are at least one order of magnitude higher.

3.1.3. Lateral distribution of adsorbed selenium and rock-forming elements

The results of the microscopic XRF measurements on petrographic thin section prepared from sample A with an initial concentration of 10^{-3} M of selenite show similar distribution of Fe, K and Se (Fig. 2 a,b,c). With scatter plots correlation was found among these elements which suggests that selenium is adsorbed on minerals containing both Fe and K, supposedly on illite as its structure is built up of $(K,H_3O)(Al,Mg,Fe)_2(Si,Al)_4O_{10}[(OH)_2,(H_2O)]$ blocks (Fig. 2 d,e,f) (Osán et al., 2014). Illite and muscovite have the same main reflection (10 Å) in powder X-ray diffraction, but illite was confirmed to be the main clay mineral in BCF by complementary methods (Németh et al., 2016). Muscovite and biotite are scarce minerals in BCF (Németh et al., 2016), therefore the simultaneous presence of Fe and K could be linked to illite.

3.1.4. Reversibility of adsorption

Based on the results of the isotopic exchange experiments (presented in Fig. S3), the adsorption of selenite onto BCF was obtained as reversible around 80–85% in the low concentration region meanwhile above 10^{-7} M equilibrium concentration the adsorption was found to be fully reversible. These findings are in-line with the Langmuir modelling of the adsorption isotherm, strong sites are dominant for the lower concentration range.

3.2. Results of through-diffusion experiment

3.2.1. Assuming a single Se species

The downstream concentration is fitted well (Fig. 3). Because the downstream concentration (up to 2×10^{-5} mol/L, Fig. 3) is much lower than the approximately constant upstream concentration (around 1×10^{-3} mol/L, Fig. 3), the VC-VC model is approximated very well by the CC-CC model. In line with expression (6), at sufficiently large times the downstream concentration is approximately a linear function of time (Fig. 3). The predicted nearly constant upstream concentration agrees roughly with the experimental data (see Fig. 3), but the predicted linear profile in the clay core does not correspond at all with the experimental data suggesting that at least two types of diffusing Se species need to be included in the model. Although the fitted downstream concentrations agree reasonably well with the experimental data, the uncertainty on the values of $D_{app,Se}$ and α_{Se} is 60–70%.

3.2.2. Assuming two Se species

The finally measured downstream concentration (see Fig. 3) is about 50% of $C_{0,fast}$ (Table 4), meaning that the entire time range cannot be fitted with the CC-CC model: unless possibly for very small times (where the quasi-stationary state is reached but also the downstream concentration is much lower than the initial concentration $C_{0,fast}$), only the VC-VC model is valid. In case the downstream concentration would have stayed all the time much lower than the upstream concentration, expression (6) shows how the shift $C_0 \rightarrow C_{0,fast}$ affects the optimal values: (i) the apparent diffusion coefficient does not change, and (ii) $\alpha\, C_0 = \alpha_{fast}\, C_{0,fast} = \alpha_{fast}\, 0.04\, C_0$ leading to $\alpha_{fast} = \alpha / 0.04 = 25\, \alpha$. This explains why (i) the ratio between $D_{app,fast}$ and D_{app} is not too far from one ($D_{app,fast} / D_{app} \approx 2$, Table 4) and (ii) much smaller than the rock capacity factors ratio ($\alpha_{fast} \approx 21.6\, \alpha$, Table 4). The fit is poor resulting in very high uncertainties (> 100%) on the values of $D_{app,fast}$ and α_{fast}, making their values not very reliable.

From $D_{app,fast}$ and α_{fast}, the bulk profile of C_{fast} in the clay can be estimated and from the difference with the experimental data, a fair fit (Fig. 3) leads to $D_{app,slow}$ and α_{slow}. It is verified that no Se_{slow} diffuses to the downstream compartment during the duration of the experiment. The predicted evolution of the upstream concentration with two species is similar as for a single Se species (Fig. 3).

The D_{app} values of both Se species differ by nearly three orders of magnitude while the difference between their rock capacity factors is much smaller (Table 4). Assuming a total porosity $\varepsilon_{tot} = 0.02$, both species are retarded. In particular, the high (inaccurate) retardation factor for Se_{fast}, supposed to be the unretarded selenate is surprising and does not seem realistic. The corresponding K_d value for Se_{slow} is much lower than the value obtained from the batch sorption experiments.

Because in the present experiment no Se_{slow} reaches the downstream compartment, an in-diffusion experiment with the same initial condition would lead to the same Se_{slow} profile at the end of the experiment. In that case, no information about Se_{fast} can be obtained: the in-diffusion experiment would have been fitted assuming a single Se species with initial concentration C_0 and the final peak would have been contributed totally to Se_{slow}. To allow a good comparison of the diffusion parameters with the in-diffusion experiment on sample P, also a fit with these same assumptions is performed on the present experiment (Table 4). Because the bulk concentration of Se_{slow} is considerably higher than that of Se_{fast} (Fig. 3), the values of the Se_{slow} diffusion parameters in both fits (considering Se_{fast} vs. not taking it into account) are assumed to be similar, which is roughly confirmed by the fit results (Table 4). The K_d-values derived from the rock capacity factor are considerably lower than those derived in the adsorption isotherm (up to 200 L/kg).

Savoye et al. (2021) found an effective diffusion coefficient around $1.9–5.3{\cdot}10^{-12}$ m^2/s for SeO_3^{2-} on COx clay. It is worth mentioning that they worked with ^{75}Se radiotracer which contained around 6% of SeO_4^{2-} (selenate). They checked the speciation in the downstream reservoir and detected the presence of selenate only. The calculation of D_e was performed from the concentration profile in the upstream/downstream reservoir. Idemitsu et al. (2016) studied the adsorption and diffusion properties of selenite on purified and compacted bentonite (Kunipia-F) which consisted of 99% montmorillonite. They reported a range for apparent diffusion coefficient as 2.5×10^{-11} to 1.9×10^{-13} m^2/s. As the rock capacity factor can be considered as ρK_d for montmorillonite (since the porosity is negligible), values measured on compacted BCF rock fall in the range measured on compacted bentonite. T. Wu et al. (2014) also studied the adsorption properties of Se(IV) species on compacted Gaomiaozi bentonite and found D_e between 3.0×10^{-12} m^2/s and 5.3×10^{-11} m^2/s depending on the dry densities and the porosity of the

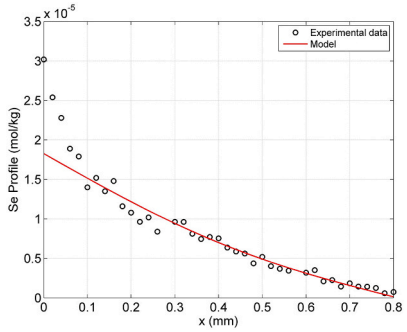

Fig. 4. In-diffusion experiment (sample P): Se profile in the clay core at the end of the experiment (data from shallow angle illumination XRF): experimental data and model assuming a single diffusing Se species (selenite).

sample (in their case the densities ranged from 1300 to 1800 kg/m^3).

3.3. Results of in-diffusion experiments

Because no breakthrough can be obtained from this type of experiment, contrary to the through-diffusion experiment, the entire Se profile in the clay core is contributed to Se_{slow}. Apart from the region very close to the upstream compartment, a good fit is obtained (Figure 4). Fitting the Se_{slow} peak of the through-diffusion experiment by totally neglecting Se_{fast}, the diffusion parameter values of both experiments differ less than a factor two (Table 4).

3.4. Oxidation state of the adsorbed Se

XANES measurements were performed on all types (thin sections, pellets pressed form adsorption experiments and compacted rock) of experiments and generally found no alteration in the spectral shapes that showed minor effect whether the system was crushed or compacted. The obtained XANES spectra are plotted in Fig. 5a. The spectra of Se(0), Na_2SeO_3 are easily distinguishable. At selected points along the diffusion axis in the in-diffusion experiment on Sample P at one point visible alteration from the previously gathered spectrum occurred. With linear combination fitting evaluation involving the spectra of Se(0) and the sum spectra of the adsorbed SeO_3 species (Characteristic spectra), approximately 23 ± 3% of selenium was found to be reduced to Se(0) (Fig. S4). Overall, under the applied atmospheric conditions the Se oxidation state did not change significantly however, at points with high pyrite content local reduction could occur. The results are in good accordance with the presumption that Na_2SeO_4 is not sorbed onto BCF. Idemitsu et al. (2016) conducted their experiments with compacted montmorillonite under both atmospheric conditions and in Ar + 5% H_2 glovebox. They found with XANES measurements that Se remained in the oxidation state of +IV during the range of their experiment. As they worked with purified bentonite, pyrite was not present in the experimental conditions. Savoye et al. (2021) worked with Opalinus Clay containing around 1% pyrite under CO_2/N_2 glovebox. They studied a rock subjected to through-diffusion experiments with μ-XRF and μ-XANES. Close to the solid-liquid interface (in the vicinity of 1 mm) they experienced no change in the XANES spectra correlated to the spectra of selenite. Deeper in the solid state the characteristic peak of the white line of Se(0) appeared around 16,660 eV. At local hot spots where Se was found to be concentrated the quantity of the reduced species emerged.

4. Conclusions

Adsorption and diffusion properties of selenite were investigated on argillaceous core samples representative of the Boda Claystone Formation. Both compacted and crushed samples were studied under atmospheric conditions. Batch experiments regarding the adsorption kinetics showed that around 10 days of solid-liquid contact was sufficient to reach equilibrium, however experiments were conducted for 28 days under atmospheric conditions. The adsorption isotherm at concentrations lower than 10^{-6} M has similar values obtained with pure clay minerals, Na-smectite and Na-illite. Above this concentration K_d started to part away from the adsorption isotherm of pure minerals and the difference gets larger with increasing equilibrium concentration. Comparing to the adsorption isotherm collected on COx similarities were found, the K_d started to decrease around 10^{-6}-10^{-7} M. The adsorption isotherm on BCF although is even lower than the one on COx, the difference is caused by the lower clay mineral content of the BCF. Langmuir isotherm fitting suggests that two different characteristics sorption sites are present in BCF. In the low concentration region the strong sites (high affinity sites) on the studied BCF sample have similar capacity to the pure minerals, but around 10^{-7} M equilibrium concentration the strong sites start to saturate similarly to other (COx, OPA) clay-rich rock samples and K_d starts decreasing. With isotopic exchange experiments the adsorption of selenite was found to be entirely reversible above 10^{-7} M equilibrium concentration. At lower concentrations (where strong sites are not saturated) the reversibility decreased to 80–85%. Microscopic X-ray fluorescence mapping showed that adsorbed selenium correlates with potassium and iron, which suggests that selenium adsorbs on clay minerals (mostly illite) on BCF.

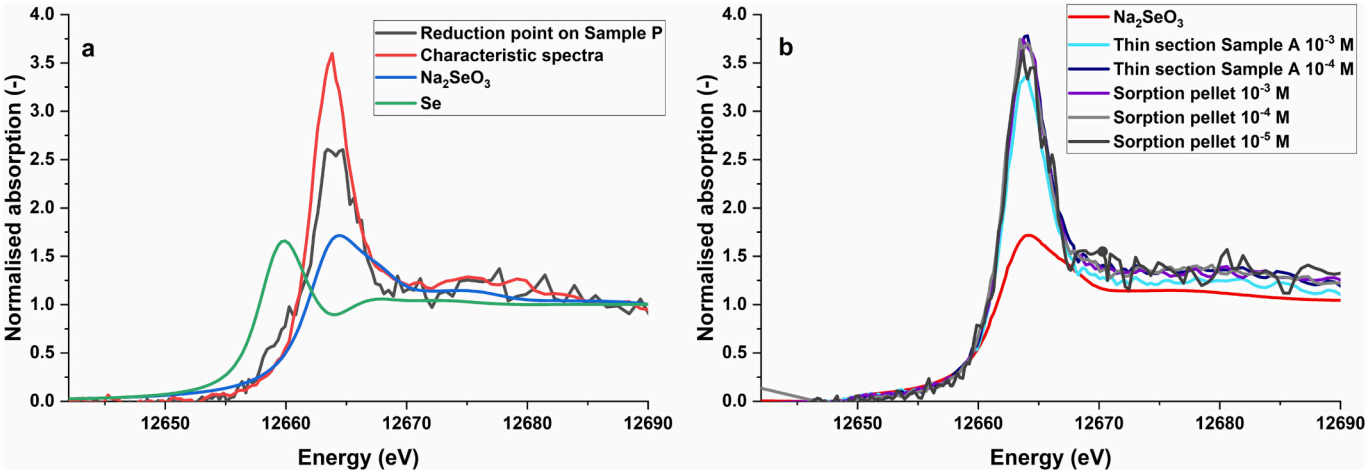

Fig. 5. XANES spectra of the sodium-selenite and the measured BCF Sample A in different forms at different concentrations (a) and the spectra showing reduction collected on in-diffusion Sample P (b).

As selenate was identified in the initial solution of diffusion experiments the through-diffusion data cannot be fitted with a single species model. The two species model roughly fits the experimental data resulting with diffusion parameters for both selenite and selenate. The obtained diffusion parameters are consistent with the values found from the in-diffusion experiment: a selenite apparent diffusion coefficient $D_{app}^{selenite} = (1.5–4.3) \times 10^{-14}$ m^2/s and a rock capacity factor $\alpha^{selenite} =$ 1.4–2.2. The selenate fit results are not reliable.

Synchrotron radiation XRF with shallow angle illumination is a promising alternative to abrasive peeling and radiotracer method for diffusion profile measurements. The mass balance of selenium had sufficiently low error (around 7%) calculated from the concentration changes in the reservoirs and the calculated adsorbed selenium content of the rock. The oxidation state of adsorption selenium remained mostly +IV, however 23% reduction at one point on a sample with high pyrite content was experienced. The retention capabilities of BCF for selenite were found to be comparable to already studied argillaceous rocks (Opalinus Clay, Callovo-Oxfordian Clay), which is an important contribution for the safety assessment of a potential deep geological repository in BCF. Because of the sensitive nature of selenium oxyanions for redox reactions, its migration properties cannot be predicted without taking into consideration the possible speciation because of the different characteristics of each form.

CRediT authorship contribution statement

O. Czömpöly: Conceptualization, Methodology, Investigation, Writing – original draft. **M. Fábián:** Investigation, Writing – review & editing. **T.I. Korányi:** Investigation. **G. Nagy:** Investigation. **Z.E. Horváth:** Investigation. **I. Zizak:** Investigation. **S. Pollastri:** Investigation, Writing – review & editing. **M. Aertsens:** Methodology, Investigation, Writing – review & editing. **J. Osán:** Conceptualization, Methodology, Investigation, Writing – review & editing, Funding acquisition.

Declaration of Competing Interest

The authors declare that they have no known competing financial interests or personal relationships that could have appeared to influence the work reported in this paper.

Data availability

Data will be made available on request.

Acknowledgement

The research was supported by the European Joint Programme on Radioactive Waste Management (EURAD) Fundamental understanding of Radionuclide Retention (FUTURE) work package (EU grant agreement number: 847593). We acknowledge Elettra Sincrotrone Trieste for providing access to its synchrotron radiation facilities and for financial support under the IUS internal project (Elettra No. 20215774 and 20220423) and acknowledge the staff of XAFS and XRF beamlines for collecting additional data during in-house beamtime. We also thank the Helmholtz-Zentrum Berlin für Materialien und Energie for the allocation of synchrotron radiation beamtime. The courtesy of the Public Limited Company for Radioactive Waste Management (PURAM, Hungary) for providing the samples for analysis is also appreciated.

Appendix A. Supplementary data

Supplementary data to this article can be found online at https://doi.org/10.1016/j.clay.2023.106997.

References

Aertsens, M., 2011. Migration in Clay: Experiments and Models SCK CEN Report SCKCEN-ER-165. SCK CEN, Mol, Belgium.

Árkai, P., Demény, A., Fórizs, I., Balogh, K., Nagy, G., Máthé, Z., 2000. Composition, diagenetic and post-diagenetic alterations of a possible radioactive waste repository site: the Boda Albitic claystone formation, southern Hungary. Acta Geol. Hung. 43 (4), 351–378.

Aurelio, G., Fernández-Martínez, A., Cuello, G.J., Román-Ross, G., Alliot, I., Charlet, L., 2010. Structural study of selenium(IV) substitutions in calcite. Chem. Geol. 270 (1–4), 249–256. https://doi.org/10.1016/J.CHEMGEO.2009.12.004.

Bailey, R.T., 2016. Review: Selenium contamination, fate, and reactive transport in groundwater in relation to human health. Hydrogeol. J. 25 (4), 1191–1217. https://doi.org/10.1007/S10040-016-1506-8.

Bradbury, M.H., Baeyens, B., 1998. A Physicochemical Characterisation and Geochemical Modelling Approach for determining Porewater Chemistries in Argillaceous Rocks. Geochim. Cosmochim. Acta 62 (5), 783–795. https://doi.org/10.1016/S0016-7037(97)00387-6.

Breitner, D., Osán, J., Fábián, M., Zagyvai, P., Szabó, C., Dähn, R., Marques Fernandes, M., Sajó, I.E., Máthé, Z., Török, S., 2015. Characteristics of uranium uptake of Boda Claystone Formation as the candidate host rock of high level radioactive waste repository in Hungary. Environ. Earth Sci. 73 (1), 209–219. https://doi.org/10.1007/S12665-014-3413-4.

Bruggeman, C., Maes, A., Vancluysen, J., Vandemussele, P., 2005. Selenite reduction in Boom clay: effect of FeS2, clay minerals and dissolved organic matter. Environ. Pollut. 137 (2), 209–221. https://doi.org/10.1016/J.ENVPOL.2005.02.010.

Dähn, R., Scheidegger, A.M., Manceau, A., Curti, E., Baeyens, B., Bradbury, M.H., Chateigner, D., 2002. Th Uptake on Montmorillonite: a Powder and Polarized Extended X-Ray Absorption Fine Structure (EXAFS) study. J. Colloid Interface Sci. 249 (1), 8–21. https://doi.org/10.1006/JCIS.2002.8236.

Dähn, R., Baeyens, B., Fernandes, M.M., 2021. Zn uptake by illite and argillaceous rocks. Geochim. Cosmochim. Acta 312, 180–193. https://doi.org/10.1016/J.GCA.2021.07.001.

De Cannière, P., Maes, A., Williams, S., Bruggeman, C., Beauwens, T., Maes, N., Cowper, M., 2010. Behaviour of Selenium in Boom Clay, External Report SCK•CEN-ER-120 10/PDC/P-9.

Descostes, M., Blin, V., Bazer-Bachi, F., Meier, P., Grenut, B., Radwan, J., Schlegel, M.L., Buschaert, S., Coelho, D., Tevissen, E., 2008. Diffusion of anionic species in Callovo-Oxfordian argillites and Oxfordian limestones (Meuse/Haute–Marne, France). Appl. Geochem. 23 (4), 655–677. https://doi.org/10.1016/J.APGEOCHEM.2007.11.003.

Fedor, F., Máthé, Z., Ács, P., Koroncz, P., 2019. New results of Boda claystone research: genesis, mineralogy, geochemistry, petrophysics. Geol. Soc. Spec. Publ. 482 (1), 75–92. https://doi.org/10.1144/SP482.13.

Frasca, B., Savoye, S., Wittebroodt, C., Leupin, O.X., Michelot, J.L., 2014. Comparative study of Se oxyanions retention on three argillaceous rocks: Upper Toarcian (Tournemire, France), Black Shales (Tournemire, France) and Opalinus Clay (Mont Terri, Switzerland). J. Environ. Radioact. 127, 133–140. https://doi.org/10.1016/J.JENVRAD.2013.10.005.

Gergely, F., Osán, J., Szabó, B.K., Török, S., 2016. Analytical performance of a versatile laboratory microscopic X-ray fluorescence system for metal uptake studies on argillaceous rocks. Spectrochim. Acta B At. Spectrosc. 116, 75–84. https://doi.org/10.1016/j.sab.2015.12.007.

He, H., Liu, J., Dong, Y., Li, H., Zhao, S., Wang, J., Jia, M., Zhang, H., Liao, J., Yang, J., Yang, Y., Liu, N., 2019. Sorption of selenite on Tamusu clay in simulated groundwater with high salinity under aerobic/anaerobic conditions. J. Environ. Radioact. 203, 210–219. https://doi.org/10.1016/J.JENVRAD.2019.03.020.

Hrabovszki, E., Tóth, E., Tóth, T.M., Máthé, Z., Schubert, F., 2020. Potential formation mechanisms of early diagenetic displacive veins in the Permian Boda Claystone Formation. J. Struct. Geol. 138, 104098 https://doi.org/10.1016/J.JSG.2020.104098.

Idemitsu, K., Kozaki, H., Yuhara, M., Arima, T., Inagaki, Y., 2016. Diffusion behavior of selenite in purified bentonite. Prog. Nucl. Energy 92, 279–285. https://doi.org/10.1016/J.PNUCENE.2015.08.012.

Karydas, A.G., Czyzycki, M., Leani, J.J., Migliori, A., Osan, J., Bogovac, M., Wrobel, P., Vakula, N., Padilla-Alvarez, R., Menk, R.H., Gol, M.G., Antonelli, M., Tiwari, M.K., Caliri, C., Vogel-Mikuš, K., Darby, I., Kaiser, R.B., IUCr., 2018. An IAEA multi-technique X-ray spectrometry endstation at Elettra Sincrotrone Trieste: benchmarking results and interdisciplinary applications. Urn 25 (1), 189–203. https://doi.org/10.1107/S1600577517016332. Issn:1600–5775.

Kläning, U.K., Sehested, K., 1986. Selenium(V). A pulse radiolysis study. J. Phys. Chem. 90 (21), 5460–5464. https://doi.org/10.1021/J100412A112/ASSET/J100412A112.FP.PNG_V03.

Konrád, G., Sebe, K., Halász, A., Babinszki, E., 2010. Sedimentology of a Permian playa lake: the Boda claystone formation, Hungary. Geologos 16 (1), 27–41. https://doi.org/10.2478/V10118-010-0002-1.

Lázár, K., Máthé, Z., Lázár, K., Máthé, Z., 2012. Claystone as a potential Host Rock for Nuclear Waste Storage. Clay Min. Nat. - Their Character. Modific. Appl. https://doi.org/10.5772/48123.

van Loon, L.R., Mibus, J., 2015. A modified version of Archie's law to estimate effective diffusion coefficients of radionuclides in argillaceous rocks and its application in safety analysis studies. Appl. Geochem. 59, 85–94. https://doi.org/10.1016/J.APGEOCHEM.2015.04.002.

Marques Fernandes, M., Vér, N., Baeyens, B., 2015. Predicting the uptake of Cs, Co, Ni, Eu, Th and U on argillaceous rocks using sorption models for illite. Appl. Geochem. 59, 189–199. https://doi.org/10.1016/J.APGEOCHEM.2015.05.006.

Mell, P., Megyeri, J., Riess, L., Máthé, Z., Hámos, G., Lázár, K., 2006. Diffusion of Sr, Cs, Co and I in argillaceous rock as studied by radiotracers. J. Radioanal. Nucl. Chem. 268 (2), 411–417. https://doi.org/10.1007/S10967-006-0178-6.

Mills, M.M., Sanchez, A.C., Boisvert, L., Payne, C.B., Ho, T.A., Wang, Y., 2023. Understanding smectite to illite transformation at elevated (>100 °C) temperature: Effects of liquid/solid ratio, interlayer cation, solution chemistry and reaction time. Chem. Geol. 615, 121214 https://doi.org/10.1016/J.CHEMGEO.2022.121214.

Missana, T., Alonso, U., García-Gutiérrez, M., 2009. Experimental study and modelling of selenite sorption onto illite and smectite clays. J. Colloid Interface Sci. 334 (2), 132–138. https://doi.org/10.1016/J.JCIS.2009.02.059.

Németh, T., Máthé, Z., Pekker, P., Dódony, I., Kovács-Kis, V., Sipos, P., Cora, I., Kovács, I., 2016. Clay mineralogy of the Boda Claystone Formation (Mecsek Mts., SW Hungary). Open Geosci. 8 (1), 259–274. https://doi.org/10.1515/GEO-2016-0024.

Nuclear Energy Agency (NEA), 2022. Clay Club Catalogue of Characteristics of Argillaceous Rocks. https://www.oecd-nea.org/jcms/pl_66401/clay-club-catalogue-of-characteristics-of-argillaceous-rocks-2022-update?utm_source=mnb&utm_medium=email&utm_campaign=March2022.

Osán, J., Kéri, A., Breitner, D., Fábián, M., Dähn, R., Simon, R., Török, S., 2014. Microscale analysis of metal uptake by argillaceous rocks using positive matrix factorization of microscopic X-ray fluorescence elemental maps. Spectrochim. Acta B At. Spectrosc. 91, 12–23. https://doi.org/10.1016/J.SAB.2013.11.002.

Puranen, A., Jonsson, M., Dähn, R., Cui, D., 2009. Immobilization of selenate by iron in aqueous solution under anoxic conditions and the influence of uranyl. J. Nucl. Mater. 392 (3), 519–524. https://doi.org/10.1016/J.JNUCMAT.2009.04.016.

Rahman, M.S., Clark, M.W., Yee, L.H., Comarmond, M.J., Payne, T.E., Burton, E.D., 2019. Effects of pH, competing ions and aging on arsenic(V) sorption and isotopic exchange in contaminated soils. Appl. Geochem. 105, 114–124. https://doi.org/10.1016/J.APGEOCHEM.2019.04.016.

Sámson, M. (Ed.), 2015. Final Report of Borehole BAF-2. PURAM, Paks (In Hungarian) Manuscript,. RHK-N-011/14.

Savoye, S., Schlegel, M.L., Frasca, B., 2021. Mobility of selenium oxyanions in clay-rich media: a combined batch and diffusion experiments and synchrotron-based spectroscopic investigation. Appl. Geochem. 128, 104932 https://doi.org/10.1016/J.APGEOCHEM.2021.104932.

Séby, F., Potin-Gautier, M., Giffaut, E., Borge, G., Donard, O.F.X., 2001. A critical review of thermodynamic data for selenium species at 25°C. Chem. Geol. 171 (3–4), 173–194. https://doi.org/10.1016/S0009-2541(00)00246-1.

Sipos, P., Németh, T., Máthé, Z., 2010. Preliminary results on the Co, Sr and Cs sorption properties of the analcime-containing rock type of the Boda Siltstone Formation. Central Eur. Geol. 53 (1), 67–78. https://doi.org/10.1556/CEUGEOL.53.2010.1.4.

Takeda, M., Nakajima, H., Zhang, M., Hiratsuka, T., 2008. Laboratory longitudinal diffusion tests: 1. Dimensionless formulations and validity of simplified solutions. J. Contam. Hydrol. 97 (3–4), 117–134. https://doi.org/10.1016/J.JCONHYD.2008.01.004.

Tertre, E., Dazas, B., Asaad, A., Ferrage, E., Grégoire, B., Hubert, F., Delville, A., Delay, F., 2021. Connecting molecular simulations and laboratory experiments for the study of time-resolved cation-exchange process in the interlayer of swelling clay minerals. Appl. Clay Sci. 200, 105913 https://doi.org/10.1016/J.CLAY.2020.105913.

Tian, Q., Guo, B., Chuaicham, C., Sasaki, K., 2020. Mechanism analysis of selenium (VI) immobilization using alkaline-earth metal oxides and ferrous salt. Chemosphere 248, 126123. https://doi.org/10.1016/J.CHEMOSPHERE.2020.126123.

Varga, A.R., Raucsik, B., Szakmány, G., Máthé, Z., 2006. Mineralogical, petrological and geochemical characteristics of the siliciclastic rock types of Boda Siltstone Formation. Bull. Hung. Geol. Soc. 136 (2), 201–232.

Varga, A.R., Szakmány, G., Raucsik, B., Máthé, Z., 2005. Chemical composition, provenance and early diagenetic processes of playa lake deposits from the Boda Siltstone Formation (Upper Permian), SW Hungary. Acta Geol. Hung. 48 (1), 49–68. https://doi.org/10.1556/AGEOL.48.2005.1.2.

Wu, H., Huang, W., Duan, Z., Luo, M., Wang, Z., Hua, R., 2020. Investigation of Se(IV) diffusion in compacted Tamusu clay by capillary method. J. Radioanal. Nucl. Chem. 324 (2), 903–911. https://doi.org/10.1007/S10967-020-07089-6.

Wu, T., Wang, H., Zheng, Q., Zhao, Y.L., van Loon, L.R., 2014. Diffusion behavior of Se (IV) and Re(VII) in GMZ bentonite. Appl. Clay Sci. 101, 136–140. https://doi.org/10.1016/J.CLAY.2014.07.028.

Zizak, I., 2016. The mySpot beamline at BESSY II. J. Large-Scale Res. Facil. 2, A102 https://doi.org/10.17815/JLSRF-2-113.